Stochastic Hydrology and Hydraulics 12 (1998) 83–96 © Springer-Verlag 1998

Fractal generation of surface area of porous media

Hongbing Sun, Manfred Koch

Abstract Many natural porous geological rock formations, as well as engineered porous structures, have fractal properties, i.e., they are self-similar over several length scales. While there have been many experimental and theoretical studies on how to quantify a fractal porous medium and on how to determine its fractal dimension, the numerical generation of a fractal pore structure with predefined statistical and scaling properties is somewhat scarcer. In the present paper a new numerical method for generating a three-dimensional porous medium with any desired probability density function (PDF) and autocorrelation function (ACF) is presented. The well-known Turning Bands Method (TBM) is modified to generate three-dimensional synthetic isotropic and anisotropic porous media with a Gaussian PDF and exponential-decay ACF. Porous media with other PDF's and ACF's are constructed with a nonlinear, iterative PDF and ACF transformation, whereby the arbitrary PDF is converted to an equivalent Gaussian PDF which is then simulated with the classical TBM. Employing a new method for the estimation of the surface area for a given porosity, the fractal dimensions of the surface area of the synthetic porous media generated in this way are then measured by classical fractal perimeter/area relationships. Different 3D porous media are simulated by varying the porosity and the correlation structure of the random field. The performance of the simulations is evaluated by checking the ensemble statistics, the mean, variance and ACF of the simulated random field. For a porous medium with Gaussian PDF, an average fractal dimension of approximately 2.76 is obtained which is in the range of values of actually measured fractal dimensions of molecular surfaces. For a porous medium with a non-Gaussian quadratic PDF the calculated fractal dimension appears to be consistently higher and averages 2.82. The results also show that the fractal dimension is neither strongly dependent of the porosity nor of the degree of anisotropy assumed.

Hongbing Sun,
Department of Geological and Marine Sciences, Rider University
2083 Lawrenceville Rd, Lawrenceville, New Jersey 08648

Manfred Koch
Department of Geohydraulics and Engineering Hydrology,
University of Kassel, Kurt-Wolters-Straße 3, 34109 Kassel

Correspondence to: Hongbing Sun e-mail: hsun@enigma.rider.edu.
The authors are grateful to Andrew F.B. Tompson for his help with the TBM program used in this paper.

1
Introduction

Numerous experimental studies of the last decade have shown that many natural porous geological rock formations, as well as engineered porous structures, such as chemical reaction columns, have fractal properties, i.e., they are self-similar or, more specifically, self-affine over several length scales (cf. Adler, 1992; Avnir et al., 1984; 1985; Bunde and Havlin, 1991; Burrough, 1989; Cox and Wang, 1993; Dullien, 1992; Hewett, 1986; Hoeksema and Kitanidis, 1985; Katz and Thompson, 1985; Krohn, 1988a; 1988b; Krohn and Thompson, 1986; Thompson, 1991; Wong, 1985; Wong et al., 1986). Loosely speaking, fractality means that the whole of a

porous conglomerate looks like very similar to its parts it is made of, or in other words, there is virtually no visual difference when zooming-in (magnifying) on a porous fractal medium (Mandelbrot, 1982). This "optical confusion" is, for example, clearly recognizable from the scanning-electron-microscopic and thin-section images of various sandstone, shales and carbonates taken at different magnifications by Krohn (1988a; 1988b) and Krohn and Thompson (1986). The studies of these authors and others (cf. Katz and Thompson, 1985; Hewett, 1986) show that the fractal, or self-similar range of a porous rock or structure, as measured, for example, by its pore surface or its pore volume, usually starts somewhere beneath the long-length, non-fractal Euclidean regime of the order of the grain size and extends over several orders of magnitude down to the very short-length regime.

Several experimental studies in which either wave-scattering- or surface adsorption techniques were used have indicated fractal regimes down even to the molecular level of the crystalls that form the porous aggregate (Avnir et al., 1984; 1985; Martin and Hurd, 1987; Wong, 1985; Wong et al., 1986; Burrough, 1989). A fractal surface structure has also been found, on a much larger scale, for many naturally occuring geological and geophysical fractures, particularly seismic fault planes (cf. Okuba and Aki, 1987) and, again, on the small scale, for ruptured metal- or rock surfaces (cf. Mandelbrot et al., 1984).

In addition to the pure geometric fractal property of the porous or fractured medium itself, which is usually quantified by the fractal dimension of its pore surface or its pore volume (see later section), numerous flow processes in a porous medium have also been found to be fractal (Feder, 1988; Adler, 1992; Dullien, 1992). The most eminent representatives of this category of porous media flow are the various phenomena of viscous fingering that can occur under specific physical conditions and the understanding of which is of practical importance in many disciplines of groundwater hydrology (cf. Koch, 1993; 1994) and, especially, in petroleum reservoir modeling (cf. Perrine, 1963; Feder, 1988). For example, in the case of immiscible velocity-driven displacement flow (water flooding of oil in a reservoir), a fractal morphology of the fingers has been observed experimentally by Nittman et al. (1985) and Maloy et al. (1985). Koch (1993) and Koch (1994), in a numerical study of the dynamics of viscous fingering that arises at a miscible interface in a density-stratified fluid in porous media (Rayleigh–Taylor instability problem), obtain also fractal patterns of the fingers, though the porous medium itself was not fractal. On the other hand, Wheatcraft and Tyler (1988) demonstrate that for a fractal porous medium, purely advective transport of a conservative tracer is also fractal.

For unsaturated or partially saturated media relationships between water content and soil porosity (Rien and Sposito, 1991a; 1991b) and between water content and both the hydraulic conductivity and the matrix potential (Toledo

et al., 1990) have been established in terms of the fractal dimension of the porous medium.

These studies demonstrate that the quantitative determination of the fractality; i.e., the fractal dimension of the porous medium, is by no means of pure theoretical interest in the fundamental physics of nature alone, but has far-reaching practical applications in general soil science and subsurface hydrology. As computer simulations of the various aspects of flow and transport in porous medium become of ever-increasing importance, so is the desire for an efficient numerical generation of test medium of certain stochastic nature, with possibly, fractal character. In spite of the many experimental and theoretical studies above, on how to quantify a fractal porous medium and on how to determine its fractal dimension, the numerical generation of a fractal pore structure with predefined statistical and scaling properties is somewhat scarcer. The statistical and numerical approach used in the present paper is based on the fact that a porous medium can be characterized by a probability density function (PDF) and an autocorrelation function (ACF). By scanning a thin section of a porous medium, the light intensity values (the brightness of the light) passing through the pores will be different from that of the edges and the solid matrices. Then, setting a threshold value, the light intensity values above the threshold will represent pores, and those below the solid grains (Quiblier, 1984). The distribution of the light intensity values in space will have an exponentially decaying ACF which, for a general anisotropic porous medium, will vary in three dimensions.

The numerical method used in the present paper for generating a three-dimensional synthetic isotropic and anisotropic porous medium with any desired PDF and ACF is based on the Turning Bands Method (TBM) (Mantoglou and Wilson, 1982; Tompson et al., 1989). By setting a threshold level in the PDF, a random porous medium of given porosity can be constructed.

The new technique proposed here can easily be implemented in large-scale stochastic simulations of flow and transport in a porous medium to numerically test some of the previously established experimental relationships between various soil properties and the fractal dimension of the porous medium.

2
Theory

2.1
The turning bands generation of a random field

The turning bands method (TBM) is a common numerical technique for generating an arbitrary Gaussian random field (Mantoglou and Wilson, 1982; Tompson et al., 1989). Starting from a normal distribution with a zero mean and specified covariance structure, the TBM generates a realization of a stationary, correlated, multi-dimensional random field by reducing a two- or three-dimensional random field simulation to a series of one-dimensional simulations carried out along a finite set of lines radiating from an origin (Fig. 1). A three-dimensional field is then generated by superposing values found from a series of one-dimensional simulations along such lines. In the following section we summarize the essential theoretical foundations of the TBM as it is necessary for the purpose of the present paper, namely the generation of a fractal porous medium.

Let $Y(x)$ be a second-order stationary anisotropic Gaussian random field with zero mean and covariance σ^2, i.e. $N(0, \sigma^2)$, that has a covariance function

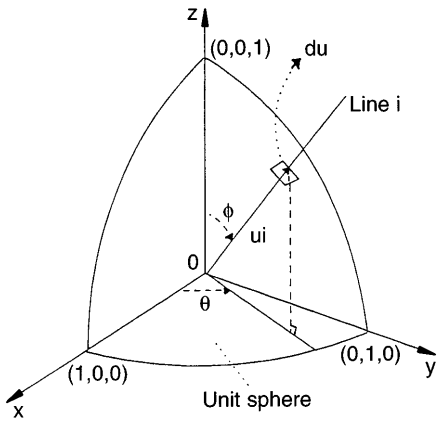

Fig. 1. Unit sphere and locations of vector **u** and the area element d**u** used in the theoretical derivation of the Turning Bands Method.

$R_{yy}(\tau) = E[Y(x)Y(x+\tau)]$, with τ the separation distance. The corresponding spectral density function $S(k)$ of the covariance is then:

$$S(k) = \frac{1}{8\pi^3}\int_{\tau} R_{yy}(\tau)\mathrm{e}^{-ik\cdot\tau}\,\mathrm{d}\tau \tag{1}$$

For the commonly used exponentially decaying anisotropic autocorrelation function

$$R_{yy}(\tau) = \sigma^2 \exp\left\{-\left(\frac{\tau_1^2}{\beta_1^2}+\frac{\tau_2^2}{\beta_2^2}+\frac{\tau_3^2}{\beta_3^2}\right)^{\frac{1}{2}}\right\} \tag{2}$$

where the β_n's are the correlation scales, the spectral density function $S(k)$ (1) will be:

$$S(k) = \frac{\sigma^2\beta_1\beta_2\beta_3}{\pi(1+k_1^2\beta_1^2+k_2^2\beta_2^2+k_3^2\beta_3^2)^2} \tag{3}$$

If one assumes a random line within the space domain, with angles θ and ϕ (Fig. 1), the line spectrum $S_l(k|\theta,\phi)$ can be shown to be related to the 3D field spectrum $S(k)$ through (Mantoglou and Wilson 1982; Tompson et al., 1989):

$$S_l(k|\theta,\phi) = 2\pi k^2 S(k) = 2\pi k^2 S(k,\theta,\phi) \tag{4}$$

One is now left with the actual generation of a random realization of the line process $Y(x)$ that has the line spectrum $S_l(k|\theta,\phi)$(4). This can be done by considering the real part of a more general, complex random process $X(x) = Y(x) + \mathrm{i}P(x)$ using the relationship:

$$X(x) = \int_{\text{all } dk} e^{ik\cdot x}\, dW(k) = \sum_{\text{all } \Delta k} e^{ik_j x}\, dW(k_j) \tag{5}$$

where, in the approximate form, X is the sum of a complex series of sinusoidal functions of varying wavelengths $K_j = j\Delta k$, each magnified by a complex random amplitude $dW(k)$ of zero mean. The latter is related to the line process $S_l(k|\theta, \phi)$ through

$$E[|dW(k))|^2] = 2S_l(k)\, dk \tag{6}$$

The real part of $X(x)$ of Eq. (5) is then:

$$Y(x) = \int_{\text{all } k} |dW(k)| \cos(k \cdot x + \phi_k) \tag{7}$$

or its discrete counterpart:

$$Y_i(x_n) = \sum_{j=0}^{M-1} |dW(k_j)| \cos(k_j x_n + \phi_j) \tag{8}$$

where ϕ_j is chosen to be a random angle distributed uniformly in [0, 2π] and magnitude:

$$|dW(k_j)| = (4S_l(k_j)\delta k)^{1/2} \tag{9}$$

The realization of the simulated field $Y_s(x)$ at a point x is then obtained from the average of all line realizations $Y_i(x, u_i)$ projected along the line with unit vector u_i:

$$Y_s(x) = \frac{1}{\sqrt{L}} \sum_{i=1}^{L} Y_i(x, u_i) \tag{10}$$

The theoretical derivations above are implemented in the TBM of Thompson et al. (1989). These authors discuss also various practical considerations of the application of the TBM, such as the proper choice of the number of lines l and the discrete frequencies k_j.

2.2
Turning band generation of a 3D pore structure

2.2.1
Porous medium with Gaussian PDF

Based on the previously discussed idea of the scanning electron microscope to experimentally measure the pore structure of a soil (Quiblier, 1984; Krohn, 1988a; 1988b; Krohn and Thompson, 1986) we define an indicator function $U(i, j, k)$ by means of a threshold value Y_0 of the TBM realization $Y_s(x)$ above which the light intensity values will represent pores, and below which they will represent solid grains:

$$U(i,j,k) = \begin{cases} 0 & Y_s(x) \le Y_0 \quad \text{pore} \\ 1 & Y_s(x) > Y_0 \quad \text{solid} \end{cases} \tag{11}$$

whereby Y_0 is chosen from the inverse F^{-1} of the normalized cumulative distribution function

$$F(Y_0) = \int_{-\infty}^{Y_0} p(\tau)\,\mathrm{d}\tau \tag{12}$$

with $p(\tau)$ the normalized Gaussian PDF

$$p(\tau) = \frac{1}{\sigma\sqrt{2\pi}} \mathrm{e}^{-\frac{\tau^2}{2\sigma^2}} \tag{13}$$

Thus, the Gaussian porous medium can be transformed by the indicator function $U(i,j,k)$ to binomial porous medium with the desired porosity structure. For example, for a medium with a porosity of 0.5 (=50%), using the standard tables of the normal distribution, $Y_0 = 0$, whereas for a porosity of 0.4 (= 40%), the corresponding threshold value will be $Y_0 = -0.255$.

2.2.2
Porous medium with a non-Gaussian PDF

The TBM is also applicable if the PDF of the porous medium does not have a Gaussian distribution. However, in such a case both the probability density function and the autocorrelation function need to be transformed before the TBM can be used. The transformation is designed in such a way that the simulated realization of a Gaussian field, after the probability transformation, will provide the desired PDF and ACF.

Assume that Z is the desired random field, and Y is the Gaussian random field, as in the previous section. Then define the following linear transformation between the two autocorrelations $R_{yy}(\tau)$ and $R_{zz}(\tau)$:

$$R_{zz}(\tau) = \sum_{m=0}^{\infty} C_m^2 R_{yy}(\tau) \tag{14}$$

where $R_{zz}(\tau)$ is the desired autocorrelation function, $R_{yy}(\tau)$ is the input autocorrelation function for the gaussian random field as in Eq. (1), which after the probability density transformation will give the desired autocorrelation function, where the coefficients C_m are given from Joshi (1974) as:

$$C_m = (m!)^{-0.5} \int_{-\infty}^{\infty} f(y) p(y) H_{\mathrm{m}}(y)\,\mathrm{d}y \tag{15}$$

where $p(y)$ is the usual Gaussian PDF function and $f(y)$ is a nonlinear inverse probability transfer function (Fig. 2) which can be calculated from (1) the cumulative normal distribution function $F(y)$

$$F(y) = \frac{1}{\sqrt{2\pi}} \int_{-\infty}^{y} \mathrm{e}^{-\tau^2}\,\mathrm{d}\tau \tag{16}$$

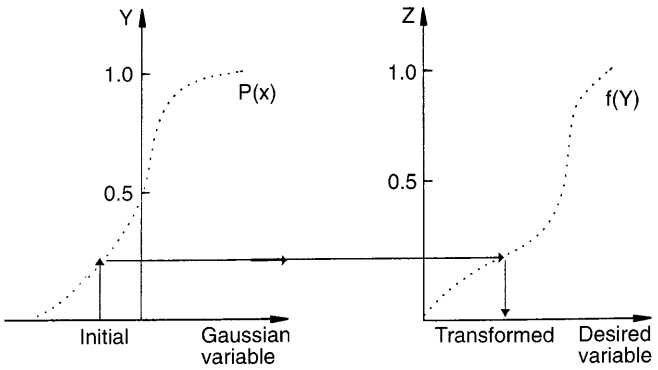

Fig. 2. Sketch showing the inverse probability transformation between a non-Gaussian and a Gaussian PDF.

and (2) the inversion of

$$F(y) = \int_0^{f(y)} p(\tau)\,\mathrm{d}\tau \tag{17}$$

where $p(\tau)$ is the desired probability density function of the realization Z. $H_m(y)$ are the Hermite polynomials which are defined recursively as:

$$H_m(y) = (-1)^{\mathrm{m}} \mathrm{e}^{y^2/2} \frac{\mathrm{d}^{\mathrm{m}}}{\mathrm{d}y^{\mathrm{m}}} \mathrm{e}^{-y^2/2} \tag{18}$$

With the transformed $R_{yy}(\tau)$, the turning bands method is then applied to simulate a gaussian random field as described above.

The algorithm developed here, based on the formulae above, consists then of the following steps:

(1) Calculation of the C_m (Eq. 15) from the measured PDF of a set of thin sections;
(2) Using the measured autocorrelation function $R_{zz}(\tau)$, calculation of the input autocorrelation function $R_{yy}(\tau)$ for the Gaussian random field simulation (Eq. 14) using an iterative Newton method;
(3) Simulation of the spatially correlated Gaussian random field with the Turning Bands Method;
(4) Calculation of the inverse probability transformation $f(y)$ (Eqs. 16 and 17) that will result in the desired spatially correlated random field with the desired PDF;
(5) Set-up of the threshold values of the light intensity according to the desired porosity (Eq. 11) and subsequent transfer of the continuous field into a discrete binomial field.

2.3
Calculation of the fractal dimension of surface area of porous media

The surface area of a synthetic porous medium can be integrated by:

$$A_a(\delta) = \sum_{i=1}^{nx} \sum_{j=1}^{ny} \sum_{k=1}^{nz} \left(\delta|_{U(i,j,k) \neq U(i+a',j+b',k+c')} \right) \tag{19}$$

where A_a is the surface area, δ is the surface area measuring scale, $U(i,j,k)$ is the porous indicator value (0,1) of Eq. (11), a', b', c' are the increments of a space point coordinate i,j,k corresponding to δ, and nx, ny, nz is the total number of grid points generated for the synthetic porous medium.

Equation (19) is implemented by choosing δ as the basic surface area measuring scale and allowing δ to "walk" through the synthetic three-dimensional sample domain. Because the surface area of the pore space in the synthetic sample is a rough surface, the measured surface area A_a should increase in form of a certain functional relationship, as the measuring scale δ is decreased. The surface area of the porous medium will then be fractal if a power-law relationship for $A_a(\delta)$ can be found.

More precisely, using the classical "coastline-divider rule" approach of Mandelbrot (1982) for a fractal object, the number-size relation between the surface area of the porous media and the measuring scale is approximately $A \sim Nr^2 \sim (r^2)^{(2-D)/2}$. Thus, it follows that

$$A_a(\delta) = a_0 \delta^{(2-D)/2} \tag{20}$$

where $A_a(\delta)$ is the surface area of pores with δ (sq. unit) area measuring scale, a_0 is the surface area when the measuring scale δ is one unit area (see below) in Eq. (20). Therefore, the fractal dimension D can be determined from the slope $\alpha = (2-D)/2$ of the logarithmic plot $A_a(\delta)$. One also notices from Eq. (20) that for a fractal dimension $D = 2$ a smooth surface will be obtained.

3. Numerical simulations and results

In order to obtain a statistical fractal dimension for the surface area of the porous media, numerous simulations are performed, whereby the correlation structure of the spatially correlated random field is varied. The performances of these simulations is checked by calculating the ensemble statistics, the mean, variance and the ACF of the simulated random porous structure. These statistical parameters provide a clue of how well the simulated field is approaching the theoretical values (Tompson et al., 1989). In order to get a reasonable statistical representation, about 30 Monte Carlo simulations for each predefined statistical distribution are carried out.

Figures 3a and 3b illustrate two typical realizations of two 3D isotropic Gaussian random porous structures with different correlation lengths β (cf. Eq. 2), namely, $\beta = (1,1,1)$ (a) and $\beta = (5,5,5)$ (b). Figure 4 shows a cross-sectional view of the $\beta = (5,5,5)$ case. A porosity of 50% is assumed for both realizations. One clearly notices the smoother, longer wavelength structure for the β = (5, 5, 5) case when compared with the case β = (1, 1, 1) of Fig. 3a.

Figure 5 depicts log-log graphs of the average measured surface area $A_a(\delta)$ for different porosities as a function of the normalized measuring scale δ (measured in standard sq. units, whereby 1 standard sq. unit is equal to 1/2500 mm^2 for the standard unit block with a volume of $1mm^3$ that is used throughout the simulations). The relatively straight lines obtained over the range of δ investigated are evidence for a fractal behavior, in accordance of Eq. (20). In addition, since the slopes of these lines are more or less identical, the fractal dimensions are invariant of the porosity assumed.

The average fractal dimension D computed from the line-slopes of Fig. 5, using Eq. (20), is approximately $D = 2.76$. This value is within the lower range

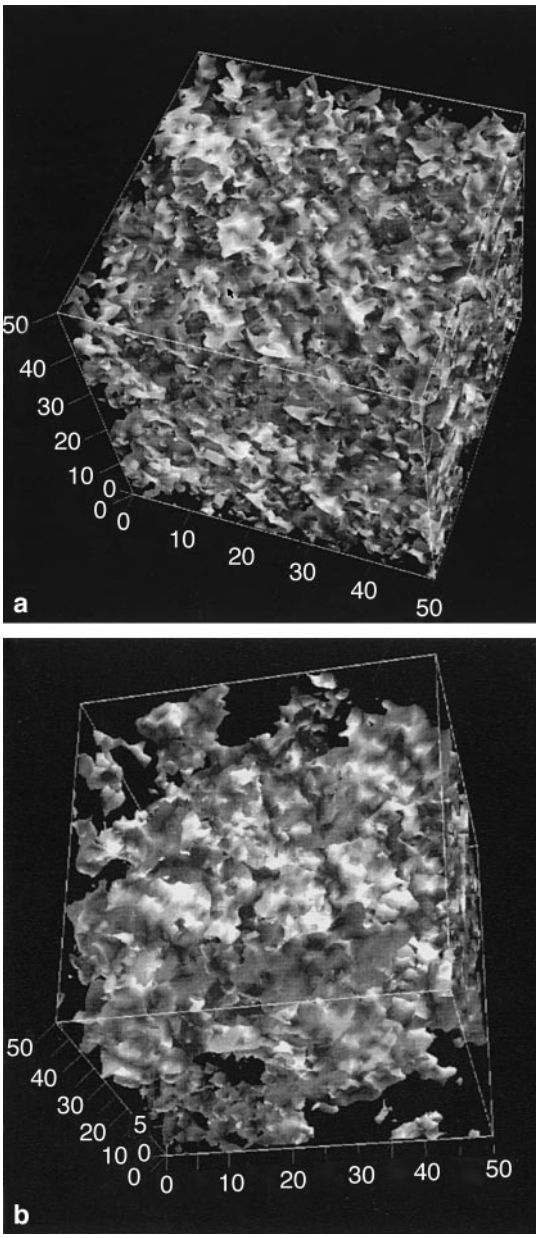

Fig. 3. Two typical realizations of two isotropic Gaussian random porous structures with different correlation lengths β; (a) $\beta = (1, 1, 1)$; (b) $\beta = (5, 5, 5)$. A 1 mm^3cubic sample with a porosity of 50% is assumed here and throughout the paper.

$(2.67 < D < 2.92)$ of fractal dimensions of porous surfaces obtained experimentally by Avnir et al. (1984) through molecular adsorption and even closer to those obtained by Krohn (1988a; 1988b) and Krohn and Thompson (1986) for various sandstone, shales and carbonates by means of scanning-electron-microscopic and thin-section images.

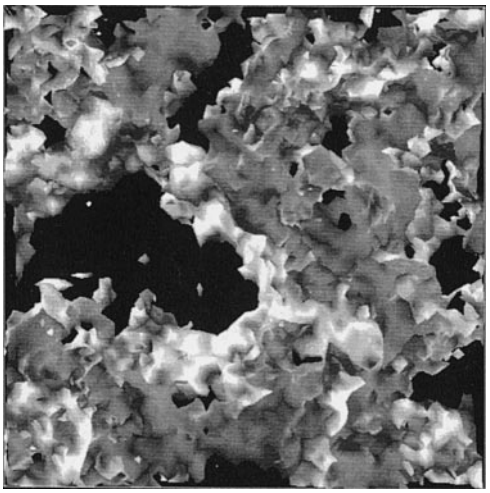

Fig. 4. Cross-sectional view of the isotropic structure β = (5,5,5) of Fig. 3b.

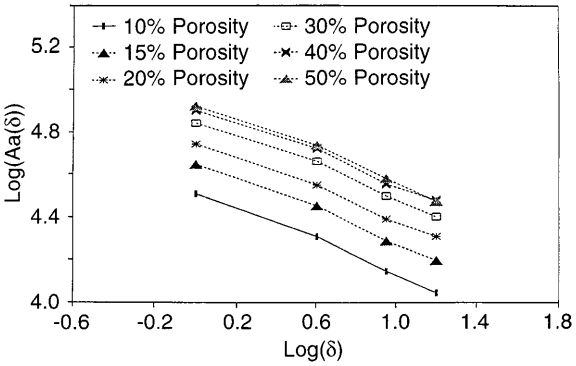

Fig. 5. Log-log plot of the measured surface area $A_a(\delta)$ as a function of the normalized measuring scale δ (see text for explanations) for different porosities of the Gaussian PDF field with an anisotropic structure, β = (1,2,3). The average fractal dimension obtained is $D = 2.76 \pm .05$.

For a porous medium with a non-Gaussian PDF, using the theory of Section 2.2.2, the fractal dimensions obtained for the surface areas can be different. For example, for realizations with a non-Gaussian, quadratic PDF $Y = (x - a)^2$ with an exponential ACF, depending on the porosities used, the fractal dimensions calculated range from $D = 2.81$ to $D = 2.85$, with an average $D = 2.82$. The corresponding log-log graphs of the surface area $A_a(\delta)$ over the normalized measuring scale δ are plotted in Fig. 6 for six different porosities. Again, the slopes of these lines are nearly equal for the various porosities assumed; i.e. the fractal dimension is rather independent of the porosity of the structure.

The fractal dimensions D obtained from numerous realizations of four Gaussian and one non-Gaussian pore structure with different correlation lengths are depicted as a function of the porosity in Fig. 7. In accordance with the statement above, the lines of D are relatively flat over the porosity-range, and D for the non-Gaussian case β = (1.9, 1.9, 1.9) is consistently higher than those D's obtained for the Gaussian structures. However, the overall range of the variations of D is only between 0.1 and 0.2.

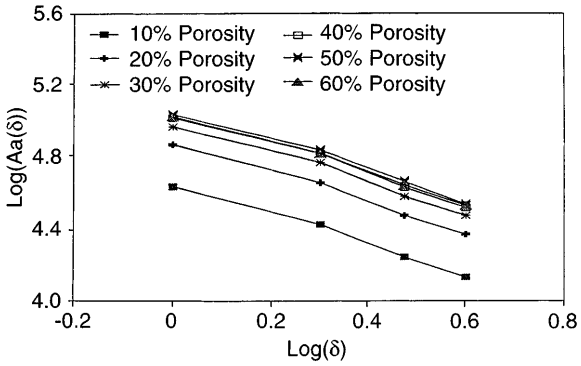

Fig. 6. Similar to Fig. 5, but for a non-Gaussian, quadratic PDF, $Y=(x\text{-}a)^2$ and an isotropic, structure, β = (1.9, 1.9, 1.9). The average fractal dimension obtained here is $D = 2.82 \pm .03$.

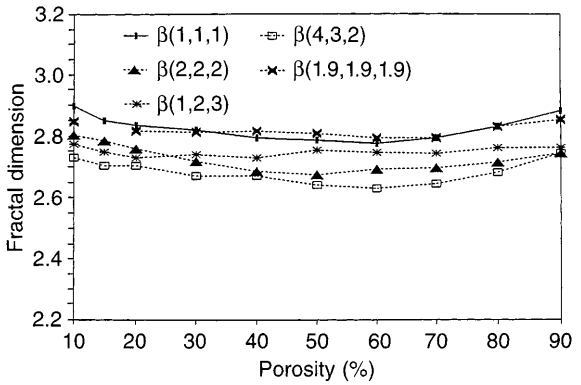

Fig. 7. Fractal dimension D versus porosity for four Gaussian and one non-Gaussian porous structures (case β=(1.9, 1.9, 1.9)). The average fractal dimension is $D = 2.76 \pm .05$ for the Gaussian structures and $D = 2.82 \pm .03$ for the non-Gaussian structure.

Figure 8 shows the changes of the surface area A_a with the porosity for various normalized measuring scales δ (see definition above) for both an isotropic (Fig. 8a) and an anisotropic (Fig. 8b) porous structure. One observes in both situations a convex functional course, whereby A_a increases gradually, as the porosity is raised from zero to 50%, and decreases hereafter monotonically again to eventually zero, as the porosity is increased further to 100% (which corresponds to an empty sample).

With the same sample volume and at the same measuring scale δ, a synthetic porous medium with a larger correlation scale β would be expected to have a smaller surface area A_a. Such a behavior is clearly illustrated in Fig. 9, and it is a quantitative manifestation of the visual appearance of the two realizations with different correlation lengths β of Fig. 3, namely, as the correlation scale increases, the matrix and pores becomes more clustered and the surface area A_a is reduced. Moreover, Fig. 9 illustrates also that an isotropic and an anisotropic porous media with the same average correlation scale β possess roughly the same surface area A_a.

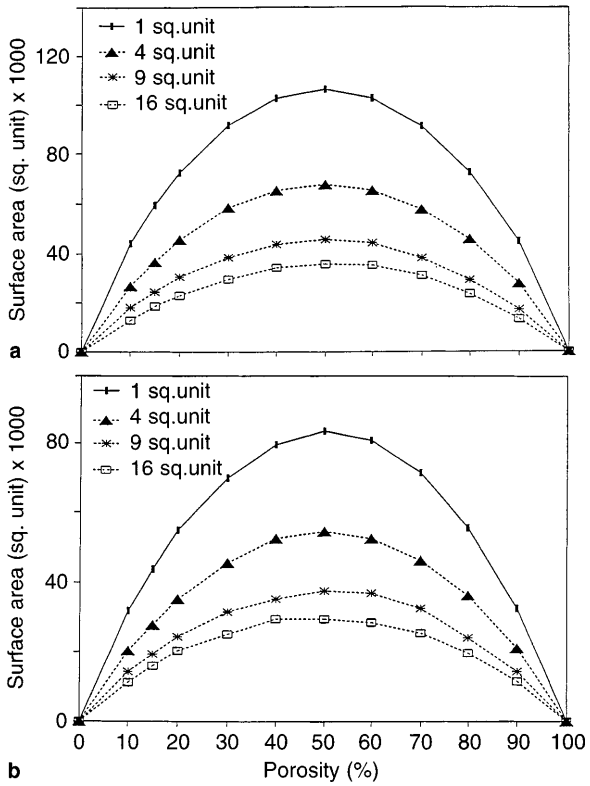

Fig. 8. Measured surface area A_a versus porosity for four different normalized measuring scales δ; a) isotropic Gaussian structure, $\beta = (1, 1, 1)$; b) anisotropic Gaussian structure. $\beta = (1, 2, 3)$.

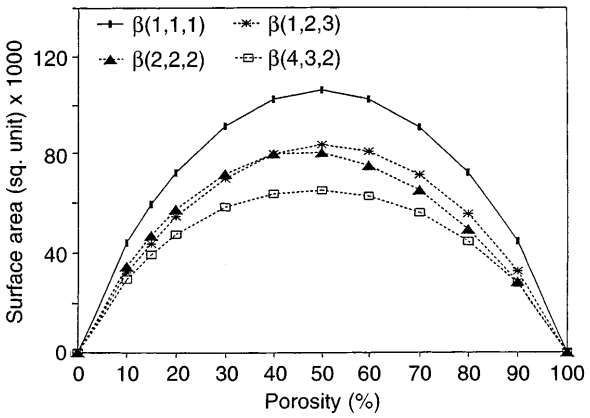

Fig. 9. Measured surface area A_a versus porosity for four Gaussian porous structures with different correlation lengths β.

4 Conclusions

One of major assets of the new method of the numerical generation of a fractal surface is that it can be applied to a three-dimensional porous medium with an

arbitrary probability density functions (PDF) and autocorrelation function (ACF). In the case of an isotropic or anisotropic porous media with a Gaussian PDF the Turning Bands Method (TBM) can be used directly. For non-Gaussian PDF with an exponential-decay ACF, the latter has to be transformed first through an inverse polynomial iteration procedure to an equivalent ACF representing a Gaussian PDF, before the TBM can be applied in the same way. Once the surface area is estimated numerically for a given porosity, its fractal dimensions are measured by classical fractal perimeter/area relationships. For a Gaussian PDF an average fractal dimension of approximately 2.76 is obtained which is in the range of values of actually measured fractal dimensions of molecular surfaces. For a porous medium with a non-Gaussian quadratic PDF the calculated fractal dimension averages 2.82. The results show that the average fractal dimension vary strongly neither with the porosity nor with the correlation length.

In spite of the versatility of the present numerical approach of the generation of a fractal porous structure for the use in Monte-Carlo type computer simulations of various aspects of flow and transport in a porous medium, several reservations are in order. The TBM program only generates stationary, homogenous porous structures with a single, uniform porosity. However, a real heterogeneous porous media may have widely different properties. The fractal properties of a porous medium of this kind can only be inferred from comparisons of numerous realizations of homogenous anisotropic synthetic medium with varied correlation structures. An accurate statistics can then be established by following the general method presented above, i.e., by simulating a large number of desired porous media structures and calculating the specific surface areas and the corresponding fractal dimensions.

References

Adler, P.M., (1992). Porous Media: Geometry and Transports, Butterworth–Heinemann Press, London

Avnir, D., Farin, D. and Pfeifer, P., (1984). Molecular fractal surfaces, Nature, 308, 261–263

Avnir, D., Farin, D. and Pfeifer, P., (1985). Surface geometric irregularity of particulate materials: The fractal approach, *J. Colloid and Interface Sci*., 103, 112–123

Bunde, A. and S. Havlin (1991). Fractals and Disordered Systems, Springer, New York, NY

Burrough, P.A., (1989). Fractals and geochemistry, in: *The Fractal Approach to Heterogeneous Chemistry*, D. Avnir (ed.), pp. 383–404, John Wiley & Sons, New York, NY

Cox, B., L. and J.S.Y. Wang (1993). Fractal surfaces: Measurement and application in the earth science, Fractals, 1, 87–115

Dullien, F. A. L., (1992). Porous Media, Fluid Transport and Pore Structure. Academic Press, Orlando, FL

Feder, J., (1988). Fractals. Plenum Press, New York, NY

Hewett, T.A., (1986). Fractal distribution of reservoir heterogeneity and their influence on fluid transport, SPE 15386, 61st Annual Technical Conference Soc. Petr. Eng., New Orleans, Oct. 5–8, 1986

Hoeksema, R.J. and P.K. Kitanidis (1985). Analysis of the spatial structure of properties of selected aquifers, Water Resour. Res., 21, 563–572

Joshi, M. Y., (1974). A class of stochastic models for porous media, Ph.D Dissertation, University of Kansas, Lawrence, KS

Katz, A.J. and A.H. Thompson (1985). Fractal sandstone pores: Implications for conductivity and pore formation, Phys. Rev. Lett., 54, 1325–1328

Koch, M., (1993). Modeling the dynamics of finger instabilities in porous media: Evidence for fractal and nonlinear system behavior, In: Advances in Hydroscience and -Engineering, Volume I, Wang, Sam S.Y. (ed.), pp. 1763–1774, Center for Computational Hydrosciene and Engineering, The University of Mississippi, Oxford, MS

Koch, M., (1994). The dynamics of density driven finger instabilities in stochastically heterogeneous porous media, In: Proceedings of the 'X International Conference on

Computational Methods in Water Resources', Heidelberg, July, 19–22, 1994, A. Peters, G. Wittum, B. Herrling, U. Meissner, C.A. Brebbia, W.G. Gray, and G.F. Pinder (eds)., Vol.1, pp. 481–488, Kluwer Academic Publishers, Dordrecht
Krohn, C.E., (1998a). Sandstone fractal and Euclidean pore volume distributions, T J. Geophys. Res., 93, 3286–3296
Krohn, C.E., (1998b). Fractal measurements of sandstone, shales and carbonates, J. Geophys. Res., 93, 3297–3305, 1988b
Krohn, C.E., and A.H. Thompson, (1986). Fractal sandstone pores: Automatic measurement using scanning-electron-microscopic images, Phys. Rev., Sect. B, 33, 6366–6374
Maloy, K., J. Feder and T. Jossang, 1985. Viscous fingering fractals in porous media, Phys. Rev. Lett., 55, 2688–269
Mandelbrot, B.B., (1982). The Fractal Geometry of Nature, W.H. Freeman and Company, San Francisco, CA
Mandelbrot, B.B., D.E. Passoja, and A.J. Pauley, (1984). Fractal character of fracture surfaces of metals, Nature, 308, 721–722
Mantoglou, A. and Wilson, J. L., (1982). The Turning Bands Method for the simulation of random fields using line generation by a spectral method, Water Resources Res., 18, 1379–1394
Martin, J.E. and Hurd, A.J., (1987). Scattering from Fractals, J. Appl. Crystallogr., 20, 61–78
Nitmann, J., G. Daccord and H.E. Stanley, (1985). Fractal growth of viscous fingers: Quantitative characterization of a fluid instability problem, Nature, 314, 141–144
Okuba, P.G and K. Aki, (1987). Fractal geometry in the San Andreas fault system, J. Geophys. Res., 92, 345–355
Perrine, R.L., (1963). A unified theory of stable and unstable miscible displacement, Soc. Pet. Eng. J., 3, 205–213
Quiblier, J.A., (1984). A New Three-Dimensional Modeling Technique for Studying Porous Media. J. Colloid and Interface Sci., 98, 84–102
Rien, M. and G. Sposito, (1991a). Fractal fragmentation, soil porosity, and soil water properties, I. Theory, Soil Sci. Soc. Am. J., 55, 1231–1238
Rien, M. and G. Sposito, (1991b). Fractal fragmentation, soil porosity, and soil water properties, II. Applications, Soil Sci. Soc. Am. J., 55, 1239–1244
Toledo, P.G. R.A. Novy, H.T. Davis and L.E. Scriven, (1990). Hydraulic conductivity of porous media at low water content, Soil Sci. Soc. Am. J., 54, 673–679
Tompson, A.F.B., Ababou, R. and Gelhar, L.W., (1989). Implementation of the three-dimensional turning bands random field generator. Water Resources Research, 25, 2227–2243
Thompson, A.H., (1991). Fractals in rock physics, Annu. Rev. Earth Planet. Sci., 19, 237–262, 1991
Wheatcraft, S.A and S.W. Tyler, (1988). An explanation of scale-dependent dispersivity in heterogenous aquifers using concepts of fractal geometry, Water Resour. Res., 24, 566–578
Wong, P.-Z., (1985). Scattering by homogeneous systems with rough internal surfaces: Porous solids and random-field Ising systems, Phys. Rev., B32, 7417–7424
Wong, P.-Z., J. Howard and J.-S. Lin, (1986). Surface roughening and the fractal nature of rocks, Phys. Rev. Lett., 57, 637–640